



UAV-borne, LiDAR-based elevation modelling: a method for improving local-scale urban flood risk assessment

Katerina Trepekli^{1,2} · Thomas Balstrøm¹ · Thomas Friberg¹ · Bjarne Fog¹ · Albert N. Allotey³ · Richard Y. Kofie³ · Lasse Møller-Jensen¹

Received: 18 January 2021 / Accepted: 24 February 2022 / Published online: 22 March 2022
© The Author(s) 2022

Abstract

In this study, we present the first findings of the potential utility of miniaturized light and detection ranging (LiDAR) scanners mounted on unmanned aerial vehicles (UAVs) for improving urban flood modelling and assessments at the local scale. This is done by generating ultra-high spatial resolution digital terrain models (DTMs) featuring buildings and urban microtopographic structures that may affect floodwater pathways (DTMbs). The accuracy and level of detail of the flooded areas, simulated by a hydrologic screening model (Arc-Malstrøm), were vastly improved when DTMbs of 0.3 m resolution representing three urban sites surveyed by a UAV-LiDAR in Accra, Ghana, were used to supplement a 10 m resolution DTM covering the region's entire catchment area. The generation of DTMbs necessitated the effective classification of UAV-LiDAR point clouds using a morphological and a triangulated irregular network method for hilly and flat landscapes, respectively. The UAV-LiDAR data enabled the identification of archways, boundary walls and bridges that were critical when predicting precise run-off courses that could not be projected using the coarser DTM only. Variations in a stream's geometry due to a one-year time gap between the satellite-based and UAV-LiDAR data sets were also observed. The application of the coarser DTM produced an overestimate of water flows equal to 15% for sloping terrain and up to 62.5% for flat areas when compared to the respective run-offs simulated from the DTMbs. The application of UAV-LiDAR may enhance the effectiveness of urban planning by projecting precisely the locations, extents and run-offs of flooded areas in dynamic urban settings.

Keywords LiDAR · UAV · Urban flooding · Arc-Malstrøm · Point cloud classification · Ghana

✉ Katerina Trepekli
atr@ign.ku.dk

¹ Department of Geosciences and Natural Resource Management, University of Copenhagen, Øster Volgade 10, 1350 Copenhagen, Denmark

² Department of Computer Sciences, University of Copenhagen, Universitetsparken 1, 2100 Copenhagen, Denmark

³ Institute for Scientific & Technological Information, Council for Scientific & Industrial Research, Cantonments, P.O. Box CT-2211, Accra, Ghana

1 Introduction

Climate variability will result in the occurrence of natural disasters that would go beyond our current socio-economic planning capacities if they extended to more intense and frequent hazards like floods (IPCC 2012; EU Directive 2007; Hoegh-Guldberg et al. 2018). Population growth, ageing infrastructure and alterations in land cover resulting from unplanned urbanization are all significant factors with greater flood damage potential (NOAA 2020).

For effective proactive management, technological developments of remote sensing observations and hydrological models may facilitate rapid flood forecasting maps aiming at predicting storm water consequences days in advance of the actual flooding, as well as identifying high-risk areas and flooding extents. However, precise flooding predictions may be hindered when using digital elevation models (DEMs) in hydrological models from outdated satellite data or data at spatial resolutions that are too coarse to identify local obstacles affecting flooding propagation.

Many hydrological studies rely solely on publicly available coarse-resolution, satellite-based DEMs (Kulp and Strauss 2019) in the form of digital terrain models (DTMs) representing the bare earth (e.g. ASTER GDEM, Nikolakopoulos et al. 2006) or digital surface models (DSMs) referring to surface elevations, including natural and man-made objects (e.g. STRM, Hensley et al. 2001). DTMs with spatial resolutions coarser than 6 m usually lead to predicted flooded areas that are unrealistically large (Wang and Zheng 2005; Cook and Merwade 2009). The application of coarse-resolution DSMs may also introduce even more inaccuracies in flood hazard modelling because metre-wide ground features can create a critical difference in simulated flooding (Leitão et al. 2016). Misrepresentations of bridges, tunnels or continuous walls in DEMs may result in biased estimates of the direction and amount of water flow by neglecting their important downstream effects on urban water resources (Sampson et al. 2012; Becek 2014). Thus, to generate more realistic surface pathways, fine-resolution DTMs (< 1 m) featuring buildings and urban microtopographic structures critical to water flow (hereafter DTMb) are required.

The application of light and detection ranging (LiDAR) technology may address this challenge by generating spatial 3D information in the form of point cloud data and extracting DTMBs of considerably finer resolution and higher vertical accuracy compared to spaceborne DEMs (Jain et al. 2018). Airborne-based LiDAR or imagery data sets are not available country- or region-wide. Also, such data are limited, especially in developing countries, and deployments of piloted aircraft surveys cannot always be commissioned at short notice (Brazier et al. 2016; Zhang and Crawford 2020). Alternatively, mobile and terrestrial LiDAR systems have been utilized to improve the vertical accuracy of topographic feature representation in DSMs as compared to those acquired by airborne systems (Turner et al. 2013; Brasington et al. 2012). However, the limited field of view of ground-based LiDAR may produce a variety of artefacts in floodwater depth grids (Fewtrell et al. 2011).

In the absence of high-quality topographic data and increased human vulnerability to flooding, the implementation of drone-borne LiDAR to generate fine-resolution DTMBs that supplement coarser DEMs could be particularly useful for precise urban planning where optimum strategies for flood protection must be site-specific (EEA 2013) and flood simulations should be kept up to date with dynamic urban growth (Perera et al. 2020).

Previous studies have pointed out the potential for predicting urban flooding at the local scale using unmanned aerial vehicle (UAV) imagery (Coveney and Roberts 2017) and the structure from motion (SfM) technique (Westoby et al. 2012). For

instance, Schumann et al. (2019) and Izumida et al. (2017) documented the utility of DSMs obtained by UAV imagery as a supplement to airborne LiDAR data sets for quantifying topographic alterations along floodplains. Yalcin (2019) used UAV imagery to derive fine-resolution DSMs for improving the performance of a hydraulic model in the absence of flood records. However, digital photogrammetry is often challenged by problems with feature definitions due to surface smoothing and difficulties when tuning the image matching algorithms in the SfM method (Priestnall et al. 2000). The precision of DTMs derived from UAV imagery depends strongly on the surface characteristics, with the largest errors occurring over dense vegetation masking the ground (Govedarica et al. 2018). This is because the SfM approach cannot create sufficient terrain points in these areas, and since high vegetation must be removed from the terrain analysis, the remaining gaps hinder the surface reconstruction (Hashemi-Beni et al. 2018). Compared to UAV photogrammetry, the point clouds generated by LiDAR scanners may facilitate the generation of more detailed information related to terrain under densely vegetated areas (Jakovljevic et al. 2019) and to microtopographic features because LiDARs can penetrate vegetation and directly provide a canopy's 3D structure.

A recent study tested the applicability of 1 m resolution DSM produced by UAV-LiDAR for simulating flood in a flat urban area (Li et al. 2021). The classification of the surveyed area into buildings, roads, terrain, woodland and grassland to generate the 1 m resolution DSM was not based on processing the retrieved UAV-LiDAR data but rather on utilizing UAV imagery where the land-use segments were produced from the maximum likelihood classification method in ArcGIS (Esri Inc. 2020). One of the main challenges in deriving DTMs for flood modelling applications from airborne, mobile or UAV-LiDAR point cloud data is their classification into terrain, vegetation, buildings and potentially important urban objects during floods, like elevated roads, bridges and boundary walls. Numerous filtering algorithms have been suggested for the classification of point clouds, such as the morphologically based (Zhang et al. 2003), slope-based (Vosselman 2000), triangular irregular networks (TIN) (Axelsson 2000) or neural networks (Jakovljevic et al. 2019), but there is no single method of classification that is applicable to all landscape types (Abdullah et al. 2012; Zhang et al. 2013).

UAV-based LiDAR technology can combine: (i) the flexibility of conducting spatially continuous, frequent, non-laborious, cost-effective surveys of near-surface remote sensing, especially in areas made inaccessible by hazardous environments; (ii) the generation of topographical data at finer spatial resolutions and ad hoc-based needs, as compared to airborne LiDAR scanners or satellite/airborne imagery; and (iii) the greater ability to penetrate vegetated surfaces compared to UAV imagery. To the authors' knowledge, the potential utility of UAV-LiDAR systems in urban flood modelling to identify local areas of high risk at centimetre resolution has not been reported.

Here, we hypothesize that fine-resolution elevation data sets from LiDAR using drones as a platform can increase the accuracy of flooding estimates at local scales in Accra, Ghana. The rapidly expanding coastal metropolitan is exposed to great flood risk during the seasonal rains (Ansah et al. 2020). Urban planning is not able to regulate settling fully to the point where local flooding can be avoided, highlighting the need to improve predicts of local flooding in order to deploy early flood control measures. To test our hypothesis, we initially evaluated the effectiveness of two conceptually different filtering algorithms to process point cloud data acquired from UAV-LiDAR surveys and produce precise DTMs of three flood-prone urban locations. We then applied a hydrologic screening model to assess storm water-induced run-off volumes and identify the areas of high flood risk. The inputs to the hydrologic screening model were: (i) a

10 m satellite-based DTM; and (ii) 0.3 m resolution DTMs generated by UAV-LiDAR surveys.

2 Materials and methods

2.1 Description of the method

The major components of the project were as follows:

- (i) Generation of precise DTMs at 0.3 m resolution in three urban sites of Accra by applying morphological-based and TIN-based algorithms to segment the point clouds derived from the UAV-LiDAR into ground, vegetation, buildings, and man-made features which may have a substantial effect on flood propagation.
- (ii) Quantification of the upstream run-off entering the UAV-surveyed sites from the surroundings by applying the Arc-Malstrøm hydrologic screening method (Balstrøm and Crawford 2018) at the full catchment scale using a 10 m DTM purchased from Airbus TM in the absence of publicly available DTMs at semi-low resolutions.
- (iii) Detection of the location, extent and depth of local landscape depressions (hereafter named bluespots) within the three sites using the fine-resolution DTMs as input to the hydrologic model and taking into account the pre-estimated upstream run-offs.
- (iv) Comparison of flood modelling results in terms of their potential to identify the extents and depths of bluespots and predict accumulated run-offs using the semi-low-resolution DTM and the fine-resolution LiDAR-generated DTMs.

To ensure accurate representation of finer-scale topographic features by the UAV-LiDAR system, randomly selected urban features within the flood-prone test areas were field-surveyed by measuring their dimensions. To assess the precision of projected flooded areas locally, an extensive field campaign documenting local flooding hot spots and the height of boundary walls raised to protect premises against the worst flood events were collected and accompanied by statements from local informants.

2.2 Study area

During the last century, Ghana has been challenged by severe flooding affecting more than 3.5 million people and costing 567 human lives (EM-DAT 2015). From 2015 to 2018, extreme rainfall events concurrent with the peak of the rainy season in the coastal metropolitan caused 164 deaths, and more than 43,000 people were displaced by damage to properties (Ansah et al. 2020; Marrengane and Croese 2020). It can be reasonably anticipated that the citizens of Accra will experience an increase in the frequency of urban flooding due to the projected increase in precipitation patterns if global warming is kept to 1.5 °C (Klutse et al. 2018), the rapid ongoing urbanization and the absence of mitigation strategies against climate extremes in general (Møller-Jensen et al. 2020).

The satellite-based DTM covered the major 29,690 ha drainage basin for the Greater Accra Metropolitan Area and 57 other minor drainage basins with outlets into the Gulf of Guinea covering an additional 16,650 ha (Fig. 1).

From 19 to 27 August 2019, aerial surveys using a UAV-LiDAR system were conducted in three local communities of Accra: (1) the Santa Maria area, a partially planned,

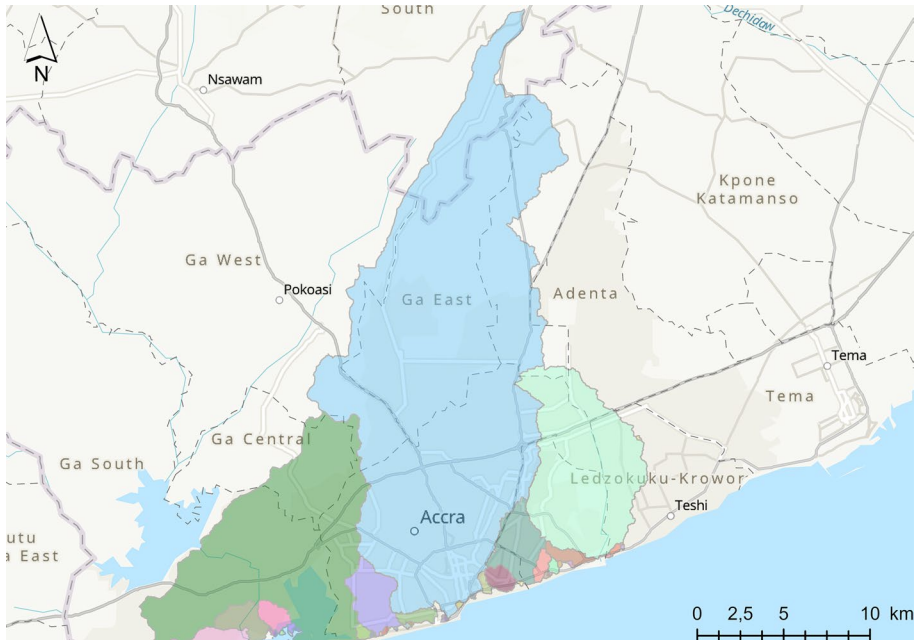


Fig. 1 Drainage basins for the Greater Accra Metropolitan Area identified from Airbus’s DTM. The main drainage basin (light blue) covers an area of 29,690 ha. The Euclidean distance from its northernmost region at Aburi to the pour point in the Gulf of Guinea is approximately 35.4 km

consolidated and densely populated settlement (2106 persons per km²) with lots of informal developments consisting of many un-engineered link roads and without properly constructed storm water drains (Oteng-Ababio et al. 2021). Flooding has been reported in key sections of roads close to a main road. The landscape includes a steep hill near the low-lying urban area; (2) The University of Ghana Campus (hereafter Legon Hall), located approximately 15 km northeast of the centre of Accra, characterized as a very flat terrain accommodating more than 40,000 people; and (3) the Okponglo flat area located in the city centre and close to Accra Sports Stadium (Fig. 2). The UAV-LiDAR surveys covered 16.7 ha at Santa Maria, 14.7 ha at Legon Hall and 25.3 ha at Okponglo.

2.3 Instrumentation

Point cloud data were acquired using a UAV-LiDAR system (LiDARSWISS, CH) onboard a Matrice 600 Pro octocopter. The LiDAR system includes an inertial navigation system (INS) that fuses data from an inertial measurement unit (OxTS micro-electro-mechanical systems) and GPS data received by a Global Navigation Satellite System (GNSS) antenna, a beam LiDAR scanner (Quanergy M8), a SONY R10-C camera with 16 mm lens, and an integrated data storage unit. The laser scanner’s horizontal field of view (FOV) is 360 degrees, and the vertical FOV is equal to 20 degrees. The heading accuracy of the laser scanner is 0.10 degrees, and the pitch/roll accuracy is equal to 0.05 degrees with an overall accuracy (RMSE) of less than 0.03 m. A Trimble Real-Time Kinematic GNSS Base Station was also used to provide additional overhead communication with the INS (approximate

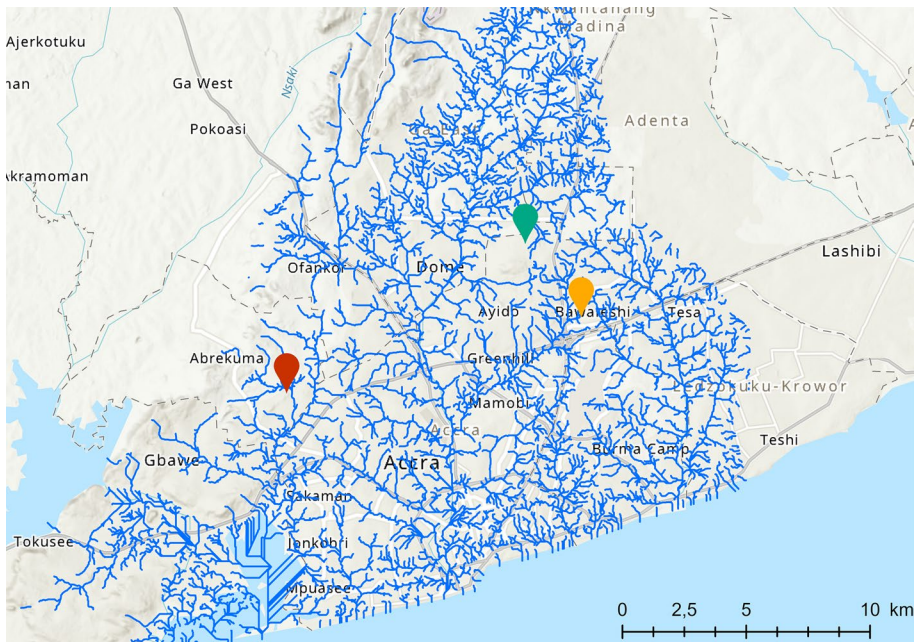


Fig. 2 Southern part of the drainage basins covering the Greater Accra Metropolitan Area and locations of the studied areas at Santa Maria (red point), Okponglo (orange point) and Legon Hall (green point)

cost 8,000 USD). The positional accuracy of the GPS receiver was 0.05 m horizontally and 0.03 m vertically. The UAV point cloud data sets were in LAS format and georeferenced to UTM WGS84 zone 30 N with a resulting mean point density equal to 60 points/m². The UAV flights with the LiDAR scanner and the digital camera onboard the drone were performed 60 m above ground with a flight speed of 5 m/s, and 80% forward overlap and 65% side overlap specifications. At Okponglo, the LiDAR data set's point spacing was 0.08 m, and the point density was 142.86 samples/m². The acquired point clouds representing the Santa Maria and Legon Hall sites had a point spacing equal to 0.05 m, and their average point densities were 471.14 and 235.17 samples/m², respectively.

2.4 Processing point cloud data to generate DTMs using the UAV-LiDAR

In this study, we assessed the effectiveness of two filtering approaches to classify the acquired point cloud data representing the hilly site of Santa Maria and the low-lying area of Okponglo (Fig. 3) using: (i) a combination of two morphological-based filters (MM) introduced by Chang et al. (2008) and Zhang et al. (2003); and (ii) the TIN algorithm. The point clouds representing the Legon Hall site were not tested since the surveyed area has a similar topography to Okponglo's and includes only a few buildings. The evaluation procedure was based on a comparison of the percentage of points grouped into different classes with the respective point clouds, manually classified through visual inspection of the derived surfaces, and with recourse to aerial imagery of the sites. Manual filtering had previously been employed to evaluate automated filter performance, as filtering errors are

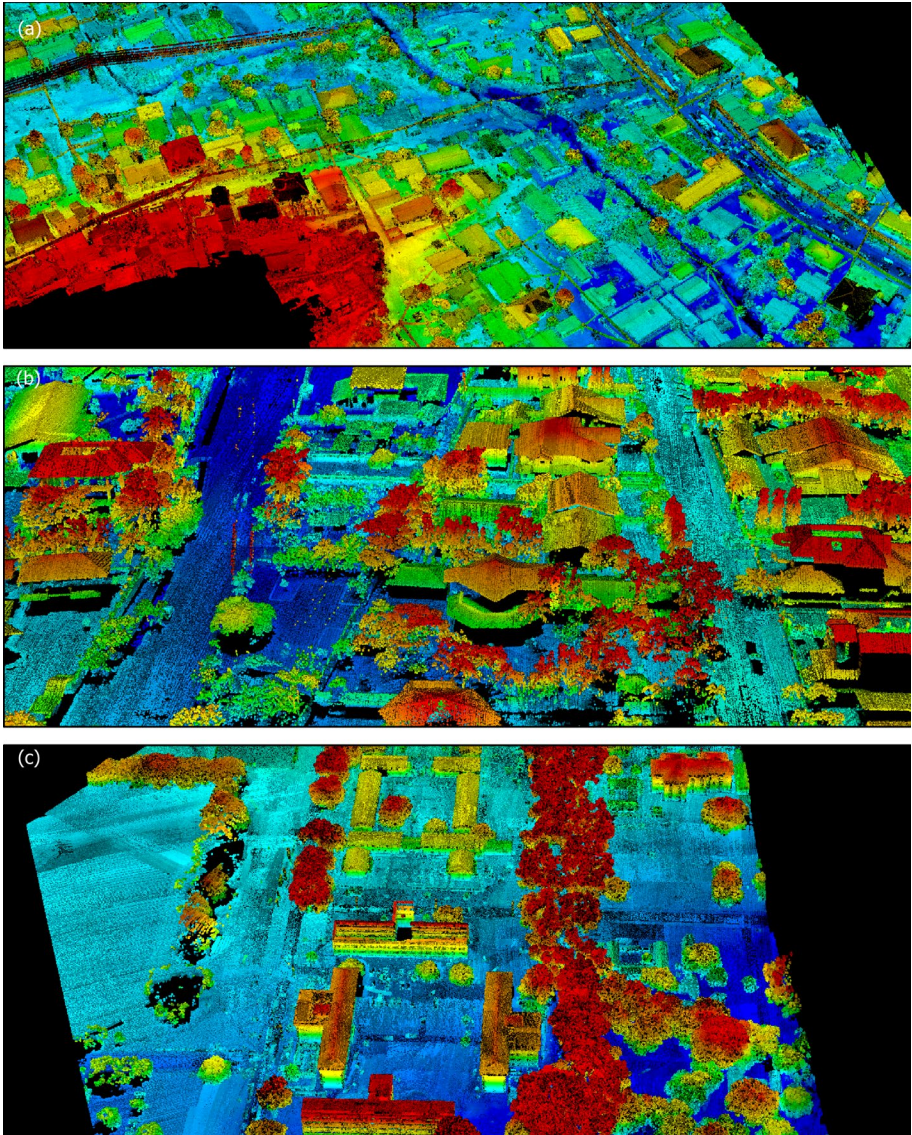


Fig. 3 Point cloud data derived by UAV-LiDAR, showing the areas of **a** Santa Maria, **b** Okponglo and **c** Legon Hall

often easy to interpret with the naked eye, and urban features are relatively easy to classify over small areas (Hutton and Brazier 2012; Sithole and Vosselman 2004).

To detect ground points, the MM filters were applied to each data set to initially remove non-ground points. The remaining points are compared with a modelled 3D curved surface within a series of grids using a multi-scale curvature algorithm. The parameterization of the morphological filters included alteration of the values for the size of the area where points are compared to their neighbours (bin size), as well as deviations of the allowed

height change from the local averaged minimum, at which points are removed from the ground classification to model a curved ground surface. The classification of buildings and trees was based on a morphological-based algorithm that relies on the points' relationship to a best-fit planar surface within each bin of the LiDAR data (Blue Marble Geographics 2020). The required minimum height above the ground for a potential building or high vegetation point was set to 1.7 m in order to include continuous boundary walls and exclude other objects like bushes and cars. Bridges were detected following the segmentation method introduced by Sithole and Vosselman (2006). The TIN refinement algorithm was applied to the LiDAR data set to perform a comparative classification of the point cloud using Rapidlasso's LAStools software. The search step size that defines the average building size and the maximal standard deviation for planar patches (i.e. building planarity and tree ruggedness) were tested to optimize the number of ground, building and tree points.

After the classification of non-ground points, objects like trees and bridges were removed to avoid water flow blocking in the storm water simulations. The remaining points were interpolated using the inverse distance weighting method (Shepard 1968) in order to rasterize the point clouds at 0.3 m resolution (DTMs).

2.5 Processing for generating satellite-based DTM

A DTM and a DSM with a grid spacing of 10 m were acquired from Airbus Defence and Space on 9 May 2018. These elevation models are generated using stereo-pair images derived by the spaceborne radar TerraSAR-X (Airbus 2017). Raw DSMs are initially generated using radargrammetry techniques based on matching homologous points from two images covering the same area. In order to reduce the influence of SAR-specific effects such as shadow or foreshortening, raw DSMs from both orbit directions are processed and merged. Voids smaller than eight pixels are interpolated, while larger voids and artefacts are filled with ancillary DSM data. For reasons of hydrological consistency, permanent water bodies are extracted, rivers and paved runways are flattened with monotonic flow to a consistent elevation, while shorelines and embankments are corrected according to the morphology of the surface as illustrated by the satellite-based images. The DTM is produced by removing the obstructions above the ground from the DSM. The voids from removing small single buildings or trees are smoothed out, while voids and artefacts in the terrain model due to the removal of larger features are interpolated. The quality control consisted of statistical assessments of the absolute and relative errors of the DEMs. The absolute accuracy describing all the random or systematic errors of a single point with respect to the horizontal and vertical datum used is expected to be within a 5 to 10 m range. The absolute horizontal accuracy of the DEMs is derived from the horizontal accuracy of the corresponding orthorectified radar image. The relative error, expressed as linear error at a 90% probability level based on the difference between processed DEMs of the same area using different acquisitions and overlapping stereo pairs, is expected to be less than 5 m.

The DTM was hydrologically corrected further using 343 digitized polylines where river underpasses or bridges along infrastructure were detected by visual inspections of Esri Basemaps. After correcting the downstream parts of the Odaw River along the industrial area of downtown Accra ($5^{\circ}34'04.3''\text{N}$ $0^{\circ}13'03.5''\text{W}$), it was observed that the river's levels had been overestimated due to an accumulation of approximately 1 million m^3 of sand, debris and largely plastic waste materials along the river and at major underpasses at the date of acquisition.

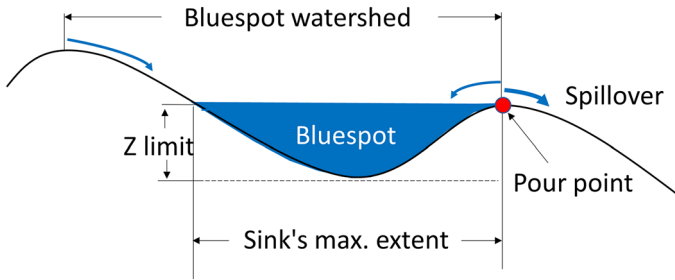


Fig. 4 Illustration of a cross section of a bluespot and the corresponding hydrological attributes that can be derived by the Arc-Malstrøm model: Bluespot's contributing watershed area (m^2), maximum depth (m), extent (m^2), capacity (m^3), or the bluespot's volume below its pour-point level, and the water loads (m^3) that enter (SpillOverIn) and exit (SpillOverOut) a bluespot for a given a uniform rain event. The SpillOverOut is calculated by the formula: $SpillOverOut = SpillOverIn + RainVolume - capacity (m^3)$

2.6 Hydrologic screening method

Two- or three-dimensional hydraulic models update flood propagation through time steps, but their computational complexity can be proportional to the resolution desired (Noh et al. 2018). The storm water screening method (Arc-Malstrøm) used in this study assumes Hortonian flow conditions and is based on a representation of the surface grouped into bluespots, their contributing local watersheds, detection of the bluespots' pour points and the streams that connect them when spilling over. When transferred to a hierarchical 1D hydrologic network, a fast-tracing operation is enabled to model the propagation of a rain event in a fast and efficient manner regardless of the resolution of the elevation model (Balstrøm and Crawford 2018). By considering a specific uniform rainfall event for the entire drainage basin, a run-off volume is calculated for each local watershed (RainVolume) that enters a bluespot. If a bluespot's capacity is reached, it produces a SpillOverOut volume at its pour point and creates a downstream water flow path (Fig. 4). If a bluespot receives water from other upstream bluespots, these spillovers are used as SpillOverIn volumes to estimate the local bluespots' water balances. Accumulated downstream spillover volumes can be derived from the individual bluespots' local water balances for a specific rain event of, say, 60 mm in such a hierarchical (topological) set-up.

The Arc-Malstrøm model was initially implemented on the entire 10 m resolution satellite-based Airbus DTM covering the entire drainage basin and considering uniform precipitation scenarios ranging from 20 to 150 mm. Then, the fine-resolution DTMbs were applied to the screening model to simulate the flood within the UAV-surveyed areas at the local scale. In the latter case, we used the run-off volumes that can be propagated within each watershed for different precipitation scenarios and the water load entering each site (SpillOverIn) from the surrounding upstream bluespots (SpillOverOut).

Identified bluespots shallower than 0.2 m and smaller than $1 m^3$ were excluded from the flood simulations in order to eliminate puddles along infrastructure and preserve deeper and more voluminous bluespots. The screening model was applied using ArcGIS Pro 2.7.0 (Esri Inc. 2020).

3 Results

3.1 Classification of point cloud data

For the low-lying flat area at Okponglo, the MM approach had a better overall performance compared to the TIN, but almost one-third of the point clouds that should have represented buildings remained unclassified (Table 1). On the other hand, the TIN approach was more effective in classifying the building points using a step size equal to 25 m and a building planarity equal to 0.1.

The optimal parameterization set for the MM approach that led to a more accurate ground classification consisted of a minimum height above the local average minimum elevation at which points were considered as non-ground equal to 0.3 m and a bin size equal to 0.5 m. The optimal RMSE from the best-fit local plane that building points must lie within was 0.2 m, with the respective minimum vegetation distance being equal to 0.3 m. For the ground classification based on the TIN approach, the 5 m step size was found to be more effective (50.27%) compared to the 25 m cell size (47.44%), but the TIN method could not identify any vegetation points (Table 1). Noticeably, the choice of an optimal step size was critical when reducing the number of faulty rejected ground points (Type I errors) and the number of faulty accepted non-ground points (Type II errors). The smaller window size preserved the terrain details, but large building features were not filtered completely, leading to high Type II errors. The larger window removed large objects effectively, but the terrain details were overlooked, leading to high Type I errors.

For the Santa Maria site, where the physical landscape is generally undulating, interspersed in most parts with plains and gentle slopes compared to the flat area at the Okponglo, the classification of point clouds was optimized using the TIN model tuned to a 5 m step size, a building planarity equal to 0.2 and a value of tree ruggedness equal to 0.4. The ground classification's performance using the MM was improved by increasing the

Table 1 Percentage of classified points and the resulting elevation range between manually classified data sets compared to the respective classified point clouds after the application of the TIN method and a combination of the slope-based and morphological-based algorithm (MM)

Site	Okponglo			Santa Maria		
	TIN	MM	References	TIN	MM	References
Ground (%)	47.44	56.25	59.47	39.2	38.37 41.47	49.85
Min elevation (m)	71.57	71.57	71.97	41.47	58	40.25
Max elevation (m)	83.27	79.82	79.70	52.69		58.51
Building/ walls (%)	20.96	12.13	25.40	21.95	34.13 43.08 54.9	50.15
Min elevation (m)	75.10 83.27	73.28	73.07	43.94		39.88
Max elevation (m)		83.27	83.34	57.37		58.51
High vegetation (%)		18.21	15.13	16.03	0.65 43.17	13.11
Min elevation (m)		73.28	73.00	43.30	54.68	42.22
Max elevation (m)		83.27	83.34	58.51		53.23
Unclassified (%)	31.59	13.32		27.91	22.06 41.8	
Min elevation (m)		71.93		41.8	58.50	
Max elevation (m)		83.27		58.51		

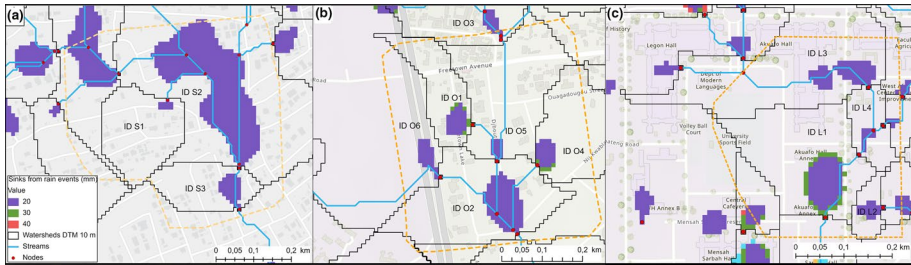


Fig. 5 Illustration of the bluespots, contributing streams and the bluespots’ local contributing watersheds as simulated using the Airbus 10 m digital terrain model (DTM) and taking into account different uniform rain events for the districts of: a) Santa Maria, b) Okponglo and c) Legon Hall. The orange dashed lines represent the area surveyed by the UAV system

Table 2 Comparison of hydrological attributes after the application of the flood model at the local scale using the DTMB generated by the UAV-LiDAR and at the urban scale using the satellite-based DTM for watersheds of the Santa Maria (S), Okponglo (O) and Legon Hall (L) sites

Watershed ID	Flood modelling at the local scale		Flood modelling at the urban scale		Difference (%) in water flow
	Water flow (m ³)	Maximum (mean) depth (m)	Water flow (m ³)	Maximum (mean) depth (m)	
S1	1211	1.63 (0.75)	1434	0.2	18.42
S2	51,522	7.59 (1.00)	58,770	1.67	14.07
S3	123,814	4.36 (1.16)	139,555	0.6	12.71
O1	128	4.7 (0.91)	208	0.58	62.5
O2	30,020	8.94 (2.44)	35,359	1.55	17.78
L1	182	12.6 (2.26)	282	1.86	54.94
L2	218	3.44 (0.63)	243	0.21	11.47

minimum height change from the local mean value to 0.5 m and by decreasing the bin size to 0.25 m, allowing for more low vegetation points to be removed.

By comparing the filtering methods’ performance in these distinctly different urban areas, it was found that the TIN approach could effectively identify the ground points in the hilly site, while the morphological-based method produced more competitive outputs in the simulated flat terrain. The resulting DTMBs of Santa Maria was based on the TIN classification (Fig. 15), while the DTMBs of the flat sites at Okponglo and Legon Hall were generated using the MM segmentation method (Figs. 16, 17).

3.2 Flood simulations using UAV-LiDAR DTMBs and semi-low-resolution elevation models

With the Arc-Malstrøm screening tool, the locations, extents and contributing watershed areas for the local bluespots were derived for the whole urban area using the Airbus 10 m DTM and visualized in a GIS environment for the three surveyed sites (Fig. 5). For each bluespot, the water depths and the accumulated water flow of the local contributing watershed area were derived assuming a 30 mm rainfall scenario (Table 2), and all detected

bluespots at the three sites were predicted to be filled and producing spillovers even after a 30 mm rain event. Interactive maps illustrating the bluespots' extent, depth, capacity, local watershed, stream network and run-off volumes for the drainage basins covering the Greater Accra Metropolitan Area are available online from the Climaccess Flood Risk Webmap Portal (2020).

The comparison of bluespots generated by the LiDAR-derived and satellite-based elevation models pointed out differences in their locations and extents within all sites. Some of the projected bluespots' locations for the Santa Maria and Okponglo sites were partially overlapped using both the semi-low and fine-resolution surface elevation models (Figs. 6, 7), but a considerable discrepancy between the locations and the extents of the bluespots generated from these approaches was visually evident for the Legon Hall site (Fig. 8).

The differences in the derived hydrological attributes in Santa Maria using the satellite-based DTM vs. the UAV-LiDAR DTMB (Fig. 6, Table 2) could also be traced to alterations to the actual topography during the time gap between the UAV-LiDAR campaign and the acquisition of Airbus's DTM (08/2019 and 05/2018, respectively). Although it could be argued that the time gap is relatively short for any significant topographical changes, we observed an alteration in the stream's course in the Santa Maria site due to reconstruction activities for a bridge at the time of the UAV-LiDAR flights, as documented by aerial photographs (see also Fig. 14). This area coincided with the simulated bluespot in Fig. 6 (orange polygon), which has a maximum depth of up to 2 m, probably due to the existence of a deep hole at the construction site. At the date, the Airbus DTM was acquired, and an

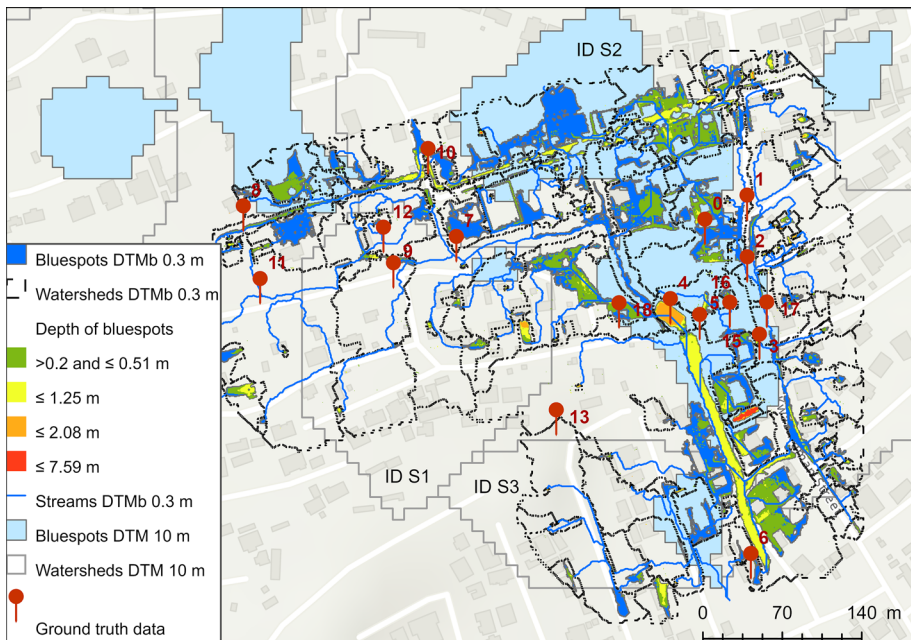


Fig. 6 Comparison of bluespot extents at the Santa Maria site as simulated by applying the semi-low-resolution DTM and the fine-resolution DTMB generated by the UAV-LiDAR. The bluespots' depths for flood modelling at the local scale were classified and coloured accordingly. Streams are represented by blue lines, watersheds by dashed black lines. Watersheds modelled at the city-wide scale (ID S1, S2 and S3) are represented by black lines

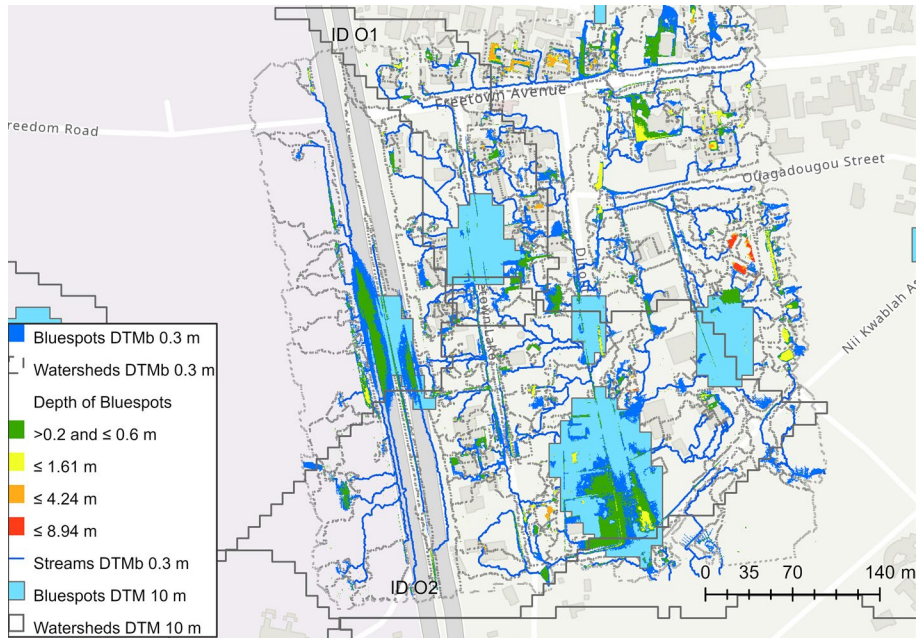


Fig. 7 Comparison of bluespot extents at the Okponglo site as simulated by applying the semi-low-resolution DTM and the fine-resolution DTMB generated by the UAV-LiDAR. The bluespots' depths for flood modelling at the local scale were classified and coloured accordingly. Streams are represented by blue lines, watersheds by dashed black lines. Watersheds modelled at the city-wide scale (ID O1, O2) are represented by black lines

immense accumulation of trash was noticed along the large Odaw River, the dislocation of concrete elements along the tamed river's walls and temporary deep holes close to construction sites in Accra city centre. Thus, the amount of water that spills from a stream on to adjacent low-lying areas could be influenced by variations in the geometry of channels and rivers resulting from human interference.

The flood map generated by the fine-resolution DTMB for Okponglo revealed the extent of filled bluespots that would occur along one major road and a secondary one in a 30 mm rain event, with a maximum bluespot depth reaching levels of 0.6 m and 1.6 m, respectively (Fig. 7). The aquaplaning locations that would pose risks to vehicle transportation during floods were also detected from the coarser DTM, but the extents of the modelled bluespots were larger. The detailed flood modelling pointed out specific buildings that could be surrounded by highly elevated precipitation run-offs. For instance, the bluespots coloured in red in Fig. 7 were considerably deep and narrow, and the resulting run-off volumes may have severe impacts on the existing infrastructure surrounded by these bluespots. This pattern was not captured by the flood modelling at the city-wide scale.

At the Legon Hall site, pathways underneath arch buildings could be identified in the LiDAR point clouds (Fig. 9). If those archways were misrepresented as continuous structures in the DTMB due to the low density of point clouds or top-view imagery, the projected stream network would be diverted, and the bluespots' locations and extents would change significantly (Fig. 10a) without maintaining the accuracy of the flood modelling (Fig. 10b).

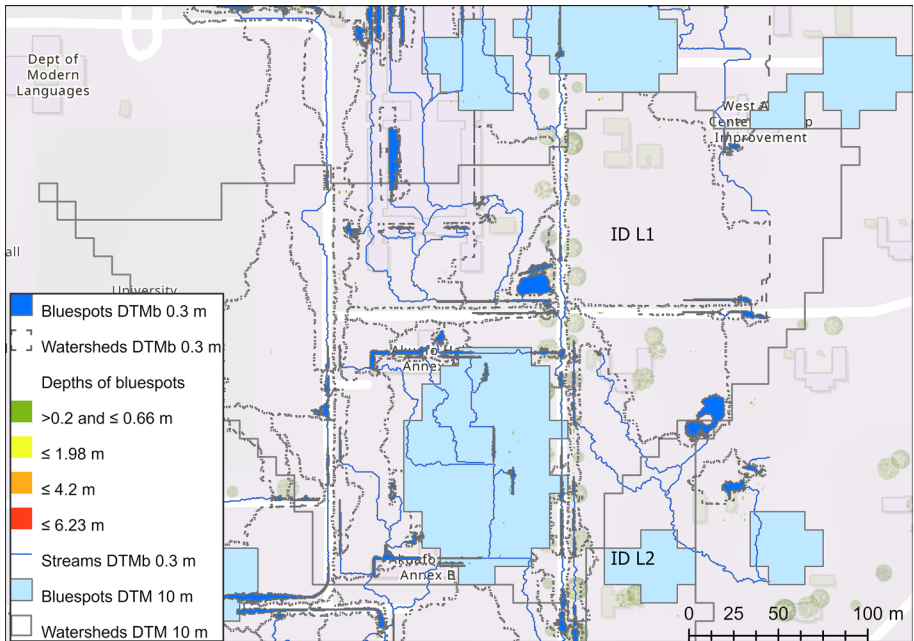


Fig. 8 Comparison of bluespot extents at the Legon Hall site as simulated by applying the semi-low-resolution DTM and the fine-resolution DTMB generated by the UAV-LiDAR. The bluespots' depths for flood modelling at the local scale were classified and coloured accordingly. Streams are represented by blue lines, watersheds by dashed black lines. Watersheds modelled at the city-wide scale (ID L1, L2) are represented by black lines

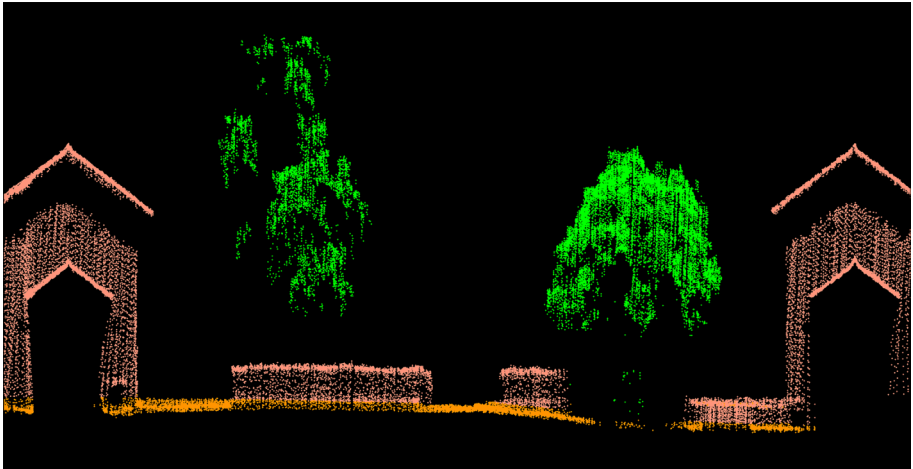


Fig. 9 Extracted point clouds representing archways, trees and concrete fences

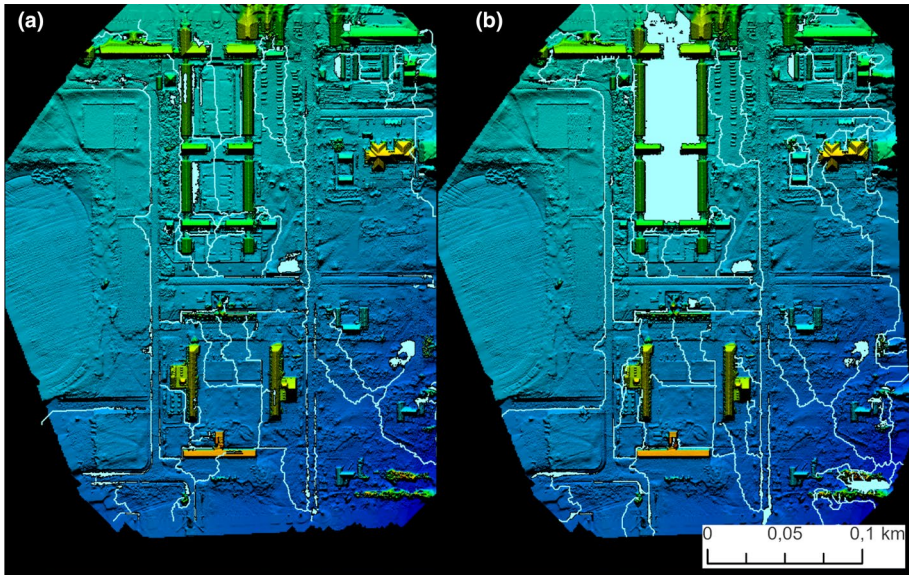


Fig. 10 Digital terrain models featuring building information and excluding vegetation (DTMb) with simulated streams and bluespots after: **a** misrepresentation of archways as buildings; and **b** preserving archways to the DTMb

3.3 Comparison of water balance attributes simulated at the urban and local scales

To assess quantitatively the effect of using finer resolution topography on the estimated water balance, the final downstream water flow calculated from the storm water simulation at the urban scale was compared with the respective total run-off simulated locally within the selected watersheds illustrated in Figs. 6, 7 and 8. Overall, the flood simulations at all sites produced shallower bluespots and larger downstream water volumes (27.41%) using the semi-low-resolution DTM (Table 2). Most likely this is an effect of the smoothing out of the Airbus' DTM's elevation values applied to remove artefacts from the DTM after subtracting above-ground objects (vegetation and buildings) from the acquired DSM in spite of the fact that the buildings should ideally have been kept to represent a DTMb in order to model the precipitation run-off around them more precisely. Under these conditions, the bluespots' capacities may be underestimated, causing more precipitation to be converted into surface run-off instead of being trapped within the bluespots. For example, the downstream water flow that spills over out of the surveyed area of Santa Maria was relatively overestimated by 12.71% due to a combination of underestimating the capacity and depth of the bluespot within ID S3 (Figs. 5, 6) and overestimating the run-off entering its watershed (i.e. the spillover vs. the downstream bluespot within ID S2).

The urban-scaled downstream water flows at the flat sites of Okponglo and Legon Hall were considerably overestimated compared to the respective water volumes simulated at the local scale using the DTMs by 62.5% and 55% for the first-order bluespots of the O1 and L1 watersheds, respectively. Similarly, Colby and Dobson (2010) stated that the flood simulations in a low-relief plain were more sensitive to the coarsening of LiDAR-derived DTMs compared to a hilly landscape.

3.4 Quantitative and qualitative validation of the hydrological modelling at the local scale

Structural information for 30 randomly selected buildings, boundary walls, bridges and containers (Fig. 18), extracted from the UAV-LiDAR point clouds, were closely correlated with field-based measurements giving the lengths and widths of the selected sample structures ($R^2=0.998$, RMSE=0.74 cm). Randomly selected point cloud data representing bridges and underpasses had correct courses when compared to the actual situation documented by aerial photographs justifying the accuracy of the UAV-LiDAR point cloud data (e.g. Fig. 11).

The ground truth points labelled 8, 10, 12 and 16 in Fig. 6 consisted of wall heights equal to 50, 100, 92 and 85 cm, respectively. In the flood simulations, these ground truth points were located within bluespots with predicted maximum depths ranging from 51 to 125 cm (Fig. 12).

Flood simulations at the local scale obtained by using fine-resolution floodplain topographic data indicated that some houses are located critically within some bluespots (Fig. 13). The qualitative testimony confirmed that floodwater regularly affects the infrastructure in this area (ground truth points 0, 3 and 6 in Fig. 6) due to spillover from a stream that was clearly outlined as an elongated bluespot. In the riparian buffer zone along the stream, extensive housing development built on or located in proximity to waterways effectively narrows the channel and impedes the free flow of water. The stream receives water from numerous small streams at uphill locations north and north-west of the studied site and merging into a low-lying valley (ground truth points 7, 8, 9 and 10). This valley contains many bluespots, and it was also highlighted as a notoriously flood-prone location by municipal officials. Field observations revealed visible evidence of road erosion caused by surface run-off in uphill areas, which provides an indication of the water volumes being carried downslope (example in Fig. 14b).

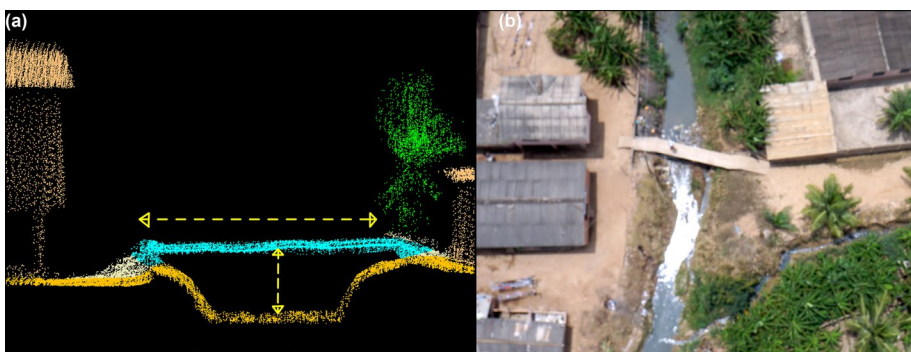


Fig. 11 Profile view of the downstream parts of a small bridge in point cloud format collected by the UAV-LiDAR and aerial view of the bridge, both collected for validating the accuracy of the point cloud



Fig. 12 Ground photographs corresponding to the ground truth points 12 and 16 in Fig. 6, where the height of the boundary walls was measured to indicate the water levels during flooding

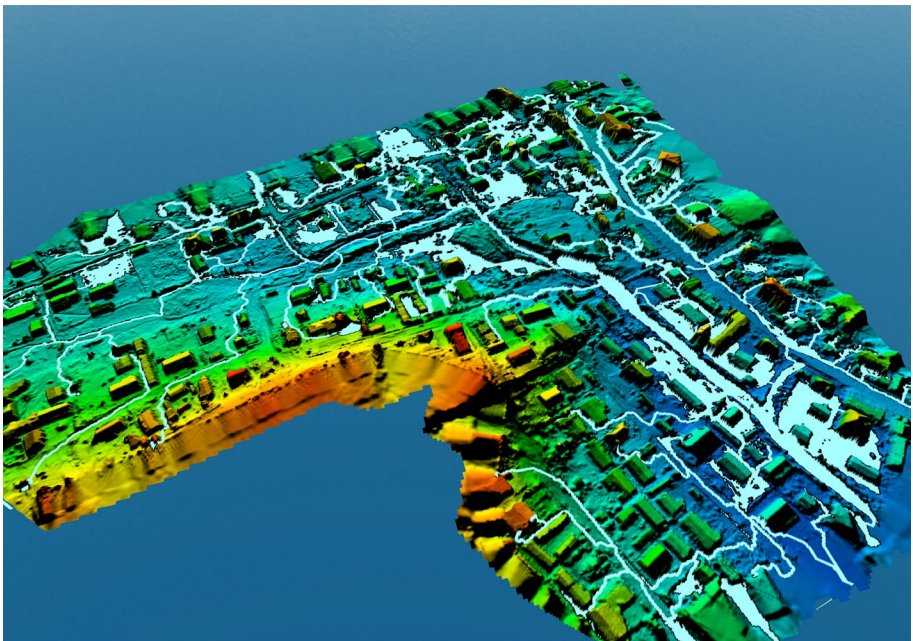


Fig. 13 A 3D view of the DTMB for the Santa Maria area surveyed by the UAV-LiDAR, showing the terrain, buildings and concrete walls. Local bluespots (polygons) and streams (lines) were simulated locally



Fig. 14 **a** Aerial photograph capturing a location where a flood-prone bridge is enlarged, causing a bluespot with a considerable depth; and **b** evidence of erosion in a partial drain due to spillover from uphill areas

4 Discussion

In this study, we have assessed the utility of UAV-LiDAR systems for simulating urban flooding locally in the absence of fine-grained topographic data by using the generated DTMs as inputs into a hydrological screening model without cutting off the links between the flood flows inside and outside these boundaries. The presented method led to increased accuracy of the flood model predictions within Accra's three local watersheds (Figs. 6; 7, Fig. 8, Table 2), showing a good degree of correspondence with physical indications of water levels (Sect. 3.4). We expect that DEMs with fine resolutions will be provided worldwide in the years to come and argue that our results demonstrate the great value of more detailed data for assessing and managing urban flood risks.

The observed differences between the locations and the extents of the bluespots generated from the coarse DTM and the fine DTMs could be attributed to underestimating the mean terrain height for each satellite-based 10 m pixel covering each surveyed area. This would consequently lead to the flooded areas' extents being overestimated. The DEMs originally produced by Airbus or publicly available satellite-based instruments (e.g. SRTM) represent the elevation of upper surfaces and not bare earth terrain. Thus, they are prone to large error with a positive bias when used to represent terrain elevations after vegetation smoothing or hydrological corrections, and this is commonly observed in densely vegetated and in densely populated areas (LaLonde et al. 2010; Shortridge and Messina 2011; Becek et al. 2014). Over- or underestimates of flow modelling may result from substantial errors in the vertical elevations (Bates 2012), but the adaptation of elevation models representing bare earth, without including man-made features (i.e. Airbus' DTM), may

also lead to biases in stream geometries. The DTMs produced by the UAV-LiDAR was able to detect bridges and pathways underneath arch buildings that affected the floodwater dynamics around urban features (Fig. 9). Similar structures can be detected using ground-view images combined with airborne LiDAR, but not necessarily using UAV photogrammetry (Meesuk et al. 2015).

DEM production and choice involves making trade-offs between accuracy, spatial coverage, cost and grid size, as well as the way they are prepared and/or corrected (Jarihani et al. 2015). Evidently, the precision of terrain characteristics that can be produced by highly dense point clouds, such as those obtained by UAV-LiDAR systems, is critical in making adequate predictions of flooded areas, particularly when the interest is focused on localized flow conditions and inundations in flood-prone areas (Zazo et al. 2015). Accra is a city with high potential for flood damage due to its urban development practices, rapid expansion and the increased frequency of heavy rainfalls, as well as its lack of topographic information. Airborne-based LiDAR data sets are currently not available, and the implementation of publicly available spaceborne DEMs (e.g. ASTER GDEM, STRM) with approximately 30 m resolution and low accuracy (Ali et al. 2015) would simply tend to increase the uncertainty of both hazard and vulnerability models (Yan et al. 2013). In addition, the footprints of buildings and other man-made urban features from the Open Street Map or from the Open Buildings Data set containing locations and building footprints across the African continent are not sufficient (e.g. Figs. 15, 16, 17) to be used as an alternative data set for generating DTMs by integrating them with semi-resolution DTMs.

However, miniaturized LiDAR onboard drones can provide a cost-effective way of capturing fine-scale spatial data (with a price starting at 40,000 USD) describing the water resource status of urban catchments and alterations of river geometry at user-defined time steps and at the local scale, the scales at which costly adaptation is usually undertaken. Thus, the fine-grained DTMs may be also relevant in flood forecasting and warning systems, where repeated and accurate topographic surveys at selected high-risk settlements are essential to detect hazards and assess the effectiveness of flood warnings to threatened localities (Popescu et al. 2015; Cools et al. 2016). Such challenges cannot be met with current satellite or airborne LiDAR/imaging survey technologies. For instance, airborne surveys using LiDAR can cover large areas offering a viable alternative to satellite-based products because they generate finer spatial resolution data with high vertical accuracy, but their high cost prohibits their use in many countries (Remondino et al. 2011). Compared to UAV imagery, UAV-LiDAR data acquisition is more flexible because the SfM method requires surveyed ground control points in order to rectify the DEMs accurately and avoid the bowl effect in the generated DEMs (Mazzoleni et al. 2020). However, there are strict flight regulations for the use of UAVs in many countries, especially over urban areas, and data acquisition is restricted by limited flight times or harsh weather conditions. Furthermore, the choice of a suitable filtering algorithm with optimized parameters may become crucial in order to retrieve the correct dimensions of the buildings and the resulting DTMs (Table 1). Ineffective filtering of vegetation from the point clouds has been documented as producing floodplain biases, highlighting the significance of evaluating the suitability of classification approaches to LiDAR data sets in order to improve the vertical accuracy of the elevation models (Cobby et al. 2001; Schumann et al. 2019).

The applicability of UAV-LiDAR systems for flood simulations was based on the implementation of a 1-D hydrological screening model that enables a fast and flexible set-up to produce descriptive flood maps, which can benefit present-day early warning systems and hazard assessments for flooding. The main advantage of the Arc-Malstrøm model is the computational efficiency of flood simulations, particularly when dealing with

fine-resolution DEMs in a full-scale urban domain (Zhao et al. 2021). Thus, by initially simulating the flooding at the city scale (Fig. 5), the flow interaction of the local UAV-LiDAR surveyed areas with the outer domain (Figs. 6, 7, 8) could be taken into account, but due to 1-D models' intrinsic neglect of time evolution and conservation of momentum, hydrographs or flow velocities could not be generated.

As implementation of 2D hydrodynamic models (Roo et al. 2002; Refsgaard et al. 1995, Sayama et al. 2012; Rasmy et al. 2019) tends to be computationally expensive, a common practice is to apply DEMs of coarse resolution to large-scale modelling (Fewtrell et al. 2008). For local-scale flood simulations, sufficiently detailed DTMs, like those acquired by UAV-LiDARs, would reasonably be expected to be handled by 2D–3D hydrodynamic models that are capable of managing 0.5 to 1 m resolution DEMs derived by airborne or terrestrial LiDAR data (Noh et al. 2018; Shen et al. 2015; Costabile et al. 2021). For example, De Sousa and Leitão (2018) simulated flood dynamics at a spatial resolution of 0.5 m in a 0.9 km² semi-urban catchment by merging airborne LiDAR DEM and DEM generated by UAV photogrammetry. Data acquisition by UAV-LiDAR on a city-wide scale would be demanding in terms of both costs and data processing capacity, but it is realistic at the sub-catchment scale, where local DTMs may be complex or rapidly changing.

Hydrodynamic models driven by advances in parallelization technology such as graphics processing units (Xia et al. 2019), remotely distributed computers (Yu et al. 2010), cloud computing (Glenis et al. 2013) and multi-core central processing units (Neal et al. 2009) may be more suitable to perform larger-scale flood inundation analyses using DEMs of 1 m resolution (Xing et al. 2019; Glenis et al. 2018). Whereas these technologies may reduce the computational costs to some extent (Guidolin et al. 2016), 2D or 3D hydrodynamic models require information related to land-use maps, drainage capacity, infiltration, rainfall, tidal level, flood depths, etc. (Glenis et al. 2018), that may not be always available. For Accra's drainage basin, there is an overwhelming scarcity of data related to past flood events, soil infiltration rates, drainage systems, groundwater levels and gauging stations for rainfall, water levels and streamflow observations. The Sentinel-1 Synthetic Aperture Radar (SAR) water body classification method introduced by Google Earth Engine (Copyright © geohackweek) was also used to detect flooded areas by comparing 10 m resolution SAR data acquired before and after thirteen extreme rain events during 2017–2019 at the city scale. This method has so far failed to generate reliable maps of water bodies plausibly due to a coarse smoothing out of the SAR imagery, meaning that comparing it with the bluespots modelled by the Arc-Malstrøm model for validation purposes is not yet achievable. In the absence of available long-term flood-related observations and the necessity for rapid assessments of flood risks, 1D hydrological models such as Arc-Malstrøm may be more suitable and sufficiently accurate to identify urban areas with a potential for high flood damage from the local to the full catchment scale (Zhao et al. 2021).

5 Conclusions

In this study, we have assessed a method for increasing the accuracy of urban flood simulations at the local scale by utilizing UAV-LiDAR technology and a storm water screening model. The presented method consisted of point cloud data processing to generate DTMs at fine resolutions and applied the Arc-Malström model at the city wide and local scales in order to identify areas potentially at high risk of flood damage.

The accuracy and level of detail of the flooded areas' extents, depths and run-offs were vastly improved when the fine-resolution (0.3 m) DTMs generated by the UAV-LiDAR system were used to supplement a semi-low (10 m)-resolution satellite-based DTM in the screening method for three urban sites in Accra.

One of the main advantages of the UAV-LiDAR system was its potential to identify urban microtopographic features such as buildings, boundary walls, bridges, vegetation and archways. Such features have a substantial influence on floodwater pathways, and their misrepresentation in DTMs could generate inaccurate water depths and flood propagation patterns. To improve the vertical accuracy of the DTMs and, consequently, the precision of flood simulations locally, the effectiveness of LiDAR-derived point cloud classification should be evaluated first. A morphological approach and a triangulated irregular network were found to be more suitable in classifying UAV-LiDAR data sets representing hilly and flat landscapes, respectively.

Alterations in stream geometries between the acquisition of satellite data and the experimental campaign were also observed, pointing to the utility of UAV-LiDAR in updating DEMs in areas that might have been undergoing topographic alterations since the last collection of elevation data sets from airborne LiDAR or satellite sensors.

When only the semi-low-resolution DTM was considered for flood analysis, the simulated bluespots were represented unrealistically as shallower and with larger extents. The respective downstream water flows were overestimated by approximately 15.10% for a hilly site and up to 62.5% for flat urban terrains when compared to the run-offs simulated using UAV-LiDAR-derived DTMs.

Flood predictions using the fine-resolution elevation data from UAV-LiDAR instrumentation are proposed as an invaluable resource and supplement to existing airborne or satellite-based products in producing flood maps. In this paper, we have shown that the finer representation of topography and complex urban features from UAV-LiDAR can increase the precision of projected flooded areas, thus allowing urban planning to be based on actual present-day conditions and securing the most detailed and most cost-effective drainage and flood protection in urban settlements at the local scale.

Appendix

See Figs. 15, 16, 17 and 18.

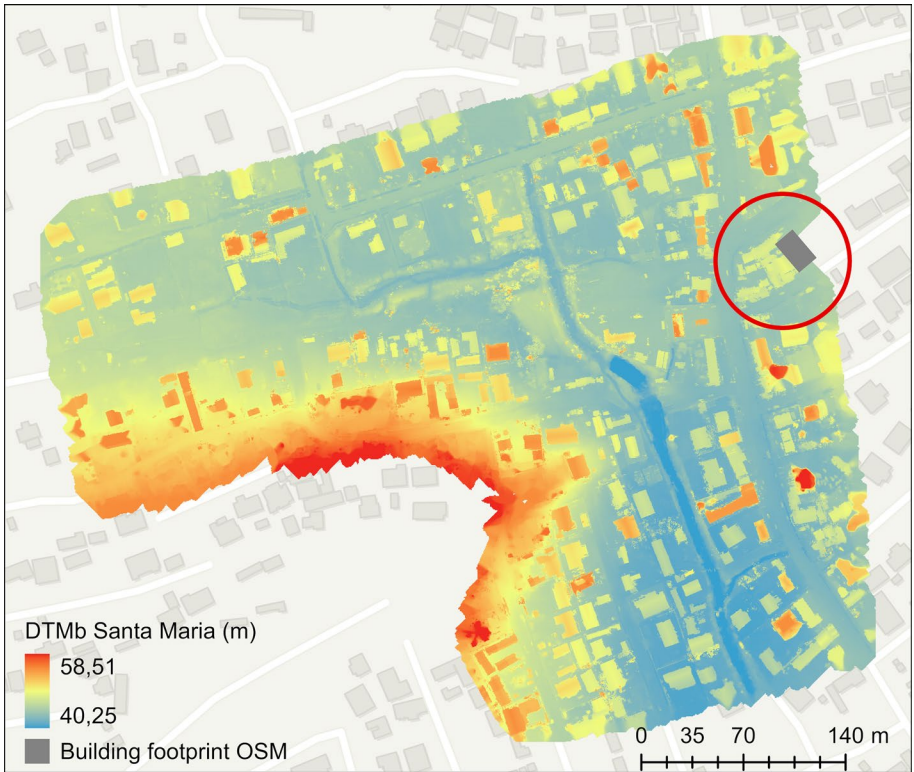


Fig. 15 DTMb (m) of the Santa Maria Site and building footprint derived from the Open Data Commons Open Database (ODbL) v1.0

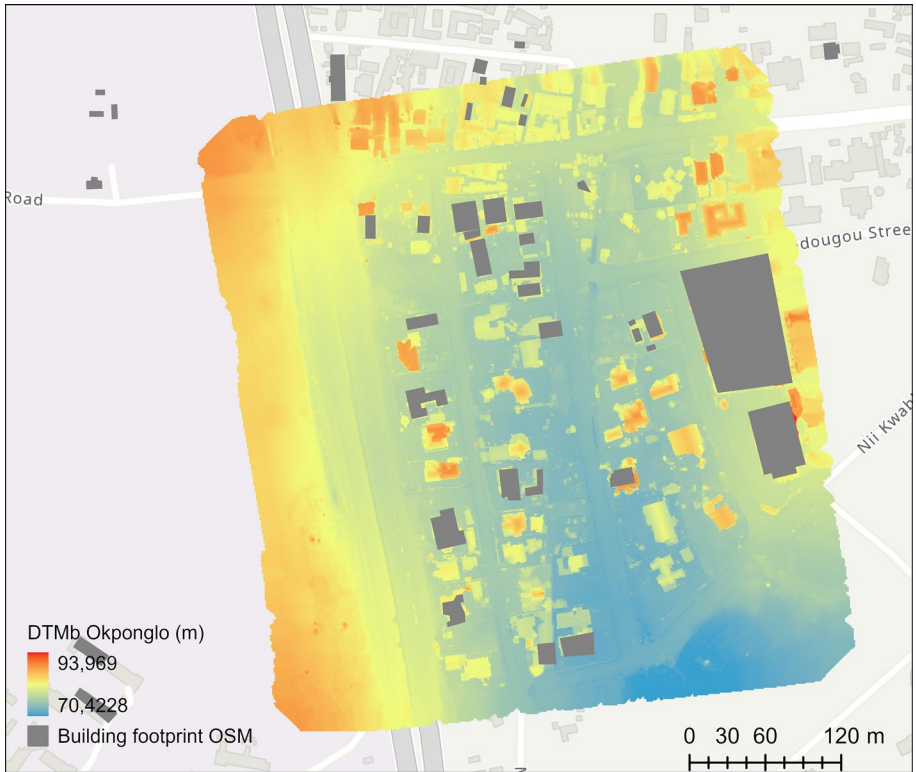


Fig. 16 DTMb (m) of the Okponglo Site and building footprint derived from the Open Data Commons Open Database (ODbL) v1.0

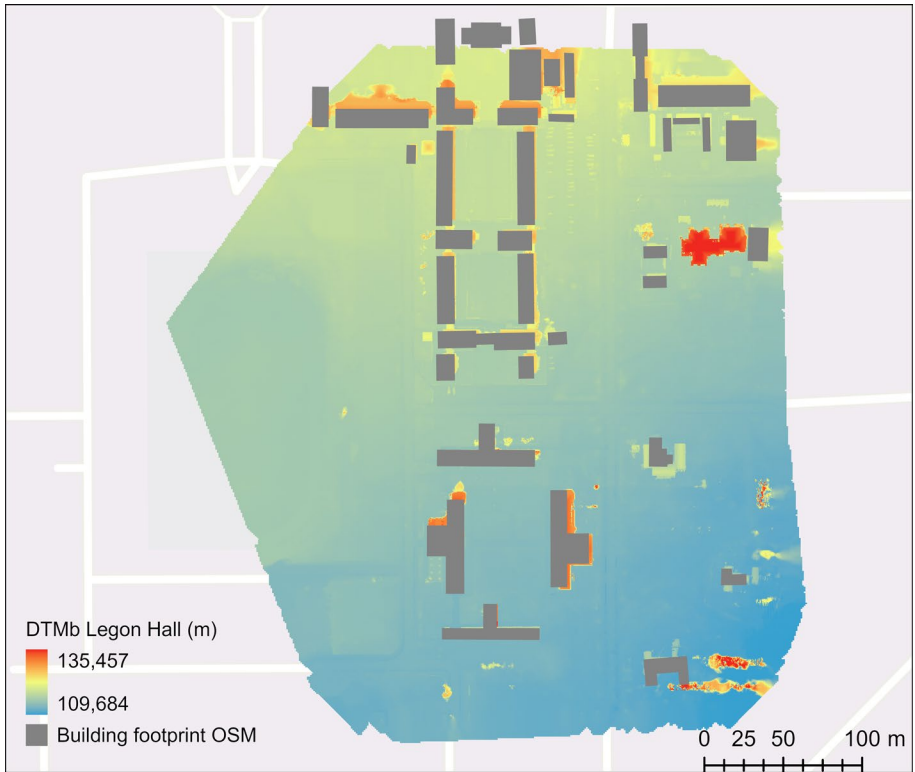


Fig. 17 DTMb (m) of the Okponglo Site and building footprint derived from the Open Data Commons Open Database (ODbL) v1.0

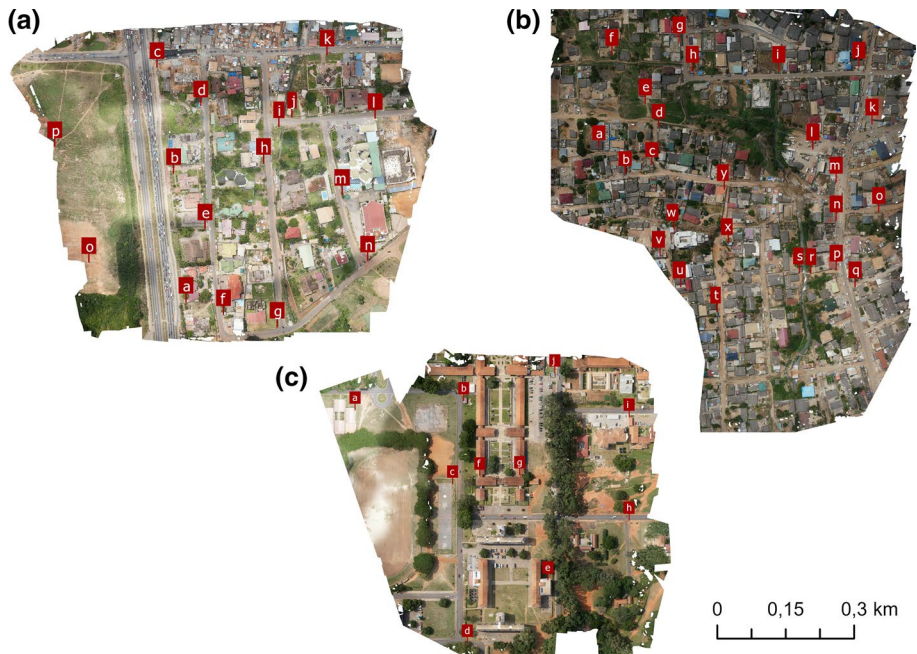


Fig. 18 Illustration of the **a** Okponglo, **b** Santa Maria and **c** Legon Hall sites surveyed by the UAV-LiDAR, indicating the locations of field-based measurements of the dimensions of man-made structures that are used to validate the accuracy of the respective point cloud data set retrieved by the UAV-LiDAR. The illustrated maps are generated using the structure-from-motion technique and images acquired from a camera integrated in the UAV-LiDAR system

Authors' contributions Lasse Møller-Jensen, Thomas Friborg, Katerina Trepekli and Bjarne Fog contributed to conceptualization; Katerina Trepekli, Thomas Balstrøm and Bjarne Fog helped in formal analysis; Katerina Trepekli, Thomas Friborg, Lasse Møller-Jensen, Albert N. Allotey and Bjarne Fog collected the data; Albert N. Allotey, Richard Y. Kofie and Lasse Møller-Jensen validated the data; Katerina Trepekli performed writing—original draft.; Thomas Balstrøm, Thomas Friborg and Lasse Møller-Jensen performed writing—review and editing.

Funding This research is being funded by a grant from the Danish Ministry of Foreign Affairs (Danida). The remote sensing equipment was funded by the UAS-ability Danish Drone Infrastructure (<https://uas-ability.dk/>).

Declarations

Conflicts of interest The authors declare no conflicts of interest.

Open Access This article is licensed under a Creative Commons Attribution 4.0 International License, which permits use, sharing, adaptation, distribution and reproduction in any medium or format, as long as you give appropriate credit to the original author(s) and the source, provide a link to the Creative Commons licence, and indicate if changes were made. The images or other third party material in this article are included in the article's Creative Commons licence, unless indicated otherwise in a credit line to the material. If material is not included in the article's Creative Commons licence and your intended use is not permitted by statutory regulation or exceeds the permitted use, you will need to obtain permission directly from the copyright holder. To view a copy of this licence, visit <http://creativecommons.org/licenses/by/4.0/>.

References

- Abdullah AF, Vojinovic' Z, Price RK, Aziz NA (2012) Improved methodology for processing raw LiDAR data to support urban flood modelling – accounting for elevated roads and bridges. *J Hydroinform* 14:253–69. <https://doi.org/10.2166/hydro.2011.009>
- Airbus Defence and Space Intelligence (2017) Elevation10 - Technical Product Specification – Version 2.3
- Ali AM, Solomatine DP, Di Baldassarre G (2015) Assessing the impact of different sources of topographic data on 1-D hydraulic modelling of floods. *Hydrol Earth Syst Sci* 19:631–643. <https://doi.org/10.5194/hess-19-631-2015>
- Ansah S, Ahiataku M, Yorke C, Otu-Larbi F, Yahaya B, Lamprey P, Tanu M (2020) Meteorological analysis of floods in Ghana. *Adv Meteorol* 2020:4230627. <https://doi.org/10.1155/2020/4230627>
- Axelsson P (2000) DEM generation from laser scanner data using adaptive TIN models. *ISPRS J Photogram Remote Sens* 33:111–118
- Balstrøm T, Crawford D (2018) Arc-Malstrøm: a 1D hydrologic screening method for storm water assessments based on geometric networks. *Comput Geosci* 116:64–73. <https://doi.org/10.1016/j.cageo.2018.04.010>
- Bates PD (2012) Integrating remote sensing data with flood inundation models: How far have we got? *Hydrol Process* 26:2515–2521. <https://doi.org/10.1002/hyp.9374>
- Beck K (2014) Assessing global digital elevation models using the runway method: the advanced spaceborne thermal emission and reflection radiometer versus the shuttle radar topography mission case. *IEEE Trans Geosci Remote Sens* 52:4823–4831. <https://doi.org/10.1109/TGRS.2013.2285187>
- Blue Marble Geographics (2020) <https://www.bluemarblegeo.com/knowledgebase/index.php> Accessed 19 November 2020
- Brasington J, Vericat D, Rychkov I (2012) Modeling river bed morphology, roughness, and surface sedimentology using high resolution terrestrial laser scanning. *Water Resour Res* 48:W11519. <https://doi.org/10.1029/2012WR012223>
- Brazier RE, Jones L, DeBell L, King N, Anderson K (2016) Water resource management at catchment scales using lightweight UAVs: Current capabilities and future perspectives. *J Unmanned Veh Syst* 4:7–30. <https://doi.org/10.1139/juvs-2015-0026>
- Chang C, Habib F, Lee C, Yom H (2008) Automatic classification of lidar data into ground and non-ground points. In: International archives of photogrammetry, remote sensing and spatial information sciences, Commission: WG IV/3, Beijing, XXXVII: Part B4.
- Climaccess Flood Risk Webmap Portal (2020) <https://cphunigis.maps.arcgis.com/apps/View/index.html?appid=0164848f6e1e460d9762d49e084710ed>
- Cobby DM, Mason DC, Davenport IJ (2001) Image processing of airborne scanning laser altimetry data for improved river flood modelling. *ISPRS J Photogramm Remote Sens* 56:121–138. [https://doi.org/10.1016/S0924-2716\(01\)00039-9](https://doi.org/10.1016/S0924-2716(01)00039-9)
- Colby JD, Dobson JG (2010) Flood modeling in the coastal plains and mountains: analysis of terrain resolution. *Nat Hazards Rev* 11:19–22. [https://doi.org/10.1061/\(ASCE\)1527-6988\(2010\)11:1\(19\)](https://doi.org/10.1061/(ASCE)1527-6988(2010)11:1(19))
- Cook A, Merwade V (2009) Effect of topographic data, geometric configuration and modeling approach on flood inundation mapping. *J Hydrol* 377:131–142. <https://doi.org/10.1016/j.jhydrol.2009.08.015>
- Cools J, Innocenti D, O'Brein S (2016) Lessons from flood early warning systems. *Environ Sci Policy* 58:117–122. <https://doi.org/10.1016/j.envsci.2016.01.006>
- Costabile P, Costanzo C, Lorenzo G, Santis R, Penna N, Macchione F (2021) Terrestrial and airborne laser scanning and 2-D modelling for 3-D flood hazard maps in urban areas: new opportunities and perspectives. *Environ Model Softw* 135:104889. <https://doi.org/10.1016/j.envsoft.2020.104889>
- Coveney S, Roberts K (2017) Lightweight UAV digital elevation models and orthoimagery for environmental applications: data accuracy evaluation and potential for river flood risk modelling. *Int J Remote Sens* 38:3159–3180. <https://doi.org/10.1080/01431161.2017.1292074>
- De Sousa LM, Leitão JP (2018) Improvements to DEM merging with r.mblend. In: C. Grueau, R. Laurini, & L. Ragia (eds.), *GISTAM 2018 - Proceedings of the 4th International Conference on Geographical Information Systems Theory, Applications and Management*. pp. 42–49. SciTePress. <https://doi.org/10.5220/00066725004200049>
- Directive 2007/60/EC of the European Parliament and of the Council of 23 October 2007 on the assessment and management of flood risks (Text with EEA relevance). <http://data.europa.eu/eli/dir/2007/60/oj> Accessed 20 October 2020
- EEA-European Environment Agency (2013) Floods: lessons about early warning. In *Late lessons from early warnings*. Report No 1/2013. Luxembourg ISBN: 978–92–9213–349–8
- EM-DAT (2015) The OFDA/CRED International Disaster Database, www.emdat.be/ - Université catholique de Louvain. <https://www.emdat.be/>. Accessed 16 October 2020

- ESRI (2020) ArcGIS Pro. Version 2.7.0. Redlands, CA: Environmental Systems Research Institute. <https://www.esri.com/en-us/arcgis/products/arcgis-pro/overview>
- Fewtrell TJ, Bates PD, Horritt M, Hunter NM (2008) Evaluating the effect of scale in flood inundation modelling in urban environments. *Hydrol Process* 22:5107–5118. <https://doi.org/10.1002/hyp.7148>
- Fewtrell TJ, Duncan A, Sampson CC, Neal JC, Bates PD (2011) Benchmarking urban flood models of varying complexity and scale using high resolution terrestrial LiDAR data. *Phys Chem Earth* 36:281–291. <https://doi.org/10.1016/j.pce.2010.12.011>
- Glenis V, Kutija V, Kilsby CG (2018) A fully hydrodynamic urban flood modelling system representing buildings, green space and interventions. *Environ Model Softw* 109:272–292. <https://doi.org/10.1016/j.envsoft.2018.07.018>
- Glenis V, McGough AS, Kutija V, Kilsby C, Woodman S (2013) Flood modelling for cities using cloud computing. *J Cloud Comp* 2:7. <https://doi.org/10.1186/2192-113X-2-7>
- Govedarica, M, Jakovljević, G, Alvarez-Taboada, F (2018) Flood risk assessment based on LiDAR and UAV points clouds and DEM. In: Proceedings of SPIE 10783, Remote Sensing for Agriculture, Ecosystems, and Hydrology XX, 107830B. <https://doi.org/10.1117/12.2513278>
- Guidolin M, Chen AS, Ghimire B, Keedwell EC, Djordjević S, Savic D (2016) A weighted cellular automata 2D inundation model for rapid flood analysis. *Environ Model Softw* 84:378–394. <https://doi.org/10.1016/j.envsoft.2016.07.008>
- Hashemi-Beni L, Jones J, Thompson G, Johnson C, Gebrehiwot A (2018) Challenges and opportunities for UAV-based digital Elevation model generation for flood-risk management: a case of Princeville. *North Carolina Sensors* 18:3843. <https://doi.org/10.3390/s18113843>
- Hensley S, Munjy R, Rosen P (2001) Interferometric synthetic aperture radar (IFSAR). Digital elevation model technologies and applications: the DEM user's manual, pp. 143–206
- Hoegh-Guldberg O, Jacob D, Taylor M et al (2018) Impacts of 1.5°C Global Warming on Natural and Human Systems. In: Global Warming of 1.5°C. In Masson-Delmotte V, Zhai P, Pörtner H et al. (ed.) An IPCC Special Report on the impacts of global warming of 1.5°C above pre-industrial levels and related global greenhouse gas emission pathways, in the context of strengthening the global response to the threat of climate change, sustainable development, and efforts to eradicate poverty. In press
- Hutton C, Brazier R (2012) Quantifying riparian zone structure from airborne LiDAR: Vegetation filtering, anisotropic interpolation, and uncertainty propagation. *J Hydrol* 442–443:36–45. <https://doi.org/10.1016/j.jhydrol.2012.03.043>
- IPCC (2012) Managing the risks of extreme events and disasters to advance Climate change adaptation. In: Field CB, Barros, V, Stocker TF, Qin, D et al. (ed.). Available from Cambridge University Press, The Edinburgh Building, Shaftesbury Road, Cambridge CB2 8RU ENGLAND, pp 582
- Izumida A, Uchiyama S, Sugai T (2017) Application of UAV-SfM photogrammetry and aerial LiDAR to a disastrous flood: repeated topographic measurement of a newly formed crevasse splay of the Kinu River, central Japan. *Nat Hazards Earth Syst Sci* 17:1505–1519. <https://doi.org/10.5194/nhess-17-1505-2017>
- Jain S, Mani P, Jain S, Prakash P, Singh V, Tullos D et al (2018) A brief review of flood forecasting techniques and their applications. *Int J River Basin Manag* 16:329–344. <https://doi.org/10.1080/15715124.2017.1411920>
- Jakovljevic G, Govedarica M, Alvarez-Taboada F, Pajic V (2019) Accuracy assessment of deep learning based classification of LiDAR and UAV points clouds for DTM creation and flood risk mapping. *Geosciences* 9:323. <https://doi.org/10.3390/geosciences9070323>
- Jarihani AA, Callow JN, McVicar TR et al (2015) Satellite-derived digital elevation model (DEM) selection, preparation and correction for hydrodynamic modelling in large, low-gradient and data-sparse catchments. *J Hydrol* 524:489–506. <https://doi.org/10.1016/j.jhydrol.2015.02.049>
- Klutse N, Vincent O, Gbobaniyi O et al (2018) Potential impact of 1.5 °C and 2 °C global warming on consecutive dry and wet days over West Africa. *Environ Res Lett* 13:055013. <https://doi.org/10.1088/1748-9326/aab37b>
- Kulp SA, Strauss BH (2019) New elevation data triple estimates of global vulnerability to sea-level rise and coastal flooding. *Nat Commun*. <https://doi.org/10.1038/s41467-019-12808-z>
- LaLonde T, Shortridge A, Messina J (2010) The influence of land cover on shuttle radar topography mission (SRTM) elevations in low relief areas. *Trans GIS* 14:461–479. <https://doi.org/10.1111/j.1467-9671.2010.01217.x>
- Leitão JP, Moy de Vitry M, Scheidegger A, Rieckermann J (2016) Assessing the quality of digital elevation models obtained from mini unmanned aerial vehicles for overland flow modelling in urban areas. *Hydrol Earth Syst Sci* 20:1637–1653. <https://doi.org/10.5194/hess-20-1637-2016>

- Li B, Hou J, Li D, Yang D, Han H, Bi X, Wang X, Hinkelmann R, Xia J (2021) Application of LiDAR UAV for high-resolution flood. *Model Water Resour Managem* 35:1433–1447. <https://doi.org/10.1007/s11269-021-02783-w>
- Marrengane N, Croese S (2020) Reframing the Urban Challenge in Africa Knowledge Co-production from the South. Taylor & Francis, eBooks
- Mazzoleni M, Paron P, Reali A, Juizo D, Manane J, Brandimarte L (2020) Testing UAV-derived topography for hydraulic modelling in a tropical environment. *Nat Hazards* 103:139–163. <https://doi.org/10.1007/s11069-020-03963-4>
- Meesuk V, Vojinovic Z, Mynett A, Abdullah A (2015) Urban flood modelling combining top-view LiDAR data with ground-view SfM observations. *Adv Water Resour* 75:105–117. <https://doi.org/10.1016/j.advwatres.2014.11.008>
- Møller-Jensen L, Allotey AN, Kofie RY, Yankson PWK (2020) A comparison of satellite-based estimates of urban agglomeration size for the Accra area. *ISPRS Int J Geo-Inf* 9:79. <https://doi.org/10.3390/ijgi9020079>
- Neal J, Fewtrell T, Trigg M (2009) Parallelisation of storage cell flood models using OpenMP. *Environ Model Softw* 24:872–877. <https://doi.org/10.1016/j.envsoft.2008.12.004>
- Nikolakopoulos KG, Kamaratakis EK, Chrysoulakis N (2006) SRTM vs ASTER elevation products: comparison for two regions in Crete, Greece. *Int J Remote Sens* 27:4819–4838. <https://doi.org/10.1080/01431160600835853>
- NOAA National Centers for Environmental Information (NCEI) U.S. Billion-Dollar Weather and Climate Disasters (2020) <https://doi.org/10.25921/stkw-7w73>
- Noh SJ, Lee J, Lee S, Kawaike K, JunSeo D (2018) Hyper-resolution 1D–2D urban flood modelling using LiDAR data and hybrid parallelization. *Environ Modell Softw* 103:131–145. <https://doi.org/10.1016/j.envsoft.2018.02.008>
- Oteng-Ababio M, Agergaard J, Andreasen MH, Møller-Jensen L (2021) Flooding in Accra: between ineffective spatial planning and climate change. Department of Geosciences and Natural Resource Management, University of Copenhagen, Climaccess Policy Brief
- Perera D, Seidou O, Agnihotri J, Mehmood H, Rasmy M (2020) Challenges and technical advances in flood early warning systems (FEWSs). In: Huang Guangwei (ed) Flood impact mitigation and resilience enhancement. IntechOpen, London. <https://doi.org/10.5772/intechopen.93069>
- Popescu D, Ichim L, Caramihale T (2015) Flood areas detection based on UAV surveillance system. In Proceedings of the 19th International Conference on System Theory, Control and Computing (ICSTCC), Cheile Gradistei, Romania
- Priestnall G, Jaafar J, Duncan A (2000) Extracting urban features from LiDAR digital surface models. *Comput Environ Urban Syst* 24:65–78. [https://doi.org/10.1016/S0198-9715\(99\)00047-2](https://doi.org/10.1016/S0198-9715(99)00047-2)
- Rasmy M, Sayama T, Koike T (2019) Development of water and energy budget-based rainfall-runoff-inundation model (WEB-RRI) and its verification in the Kalu and Mundeni river basins, Sri Lanka. *J of Hydrol* 579:124–163. <https://doi.org/10.1016/j.jhydrol.2019.124163>
- Refsgaard JC, Storm K (1995) Mike she. In: Singh VP (ed) Computer models of watershed hydrology. Water Resources Publications, Colorado, USA, pp 809–846
- Remondino F, Barazzetti L, Nex F, Scaioni M, Sarazzi D (2011) UAV photogrammetry for mapping and 3D modeling-current status and future perspectives. *ISPRS Int Arch Photogramm Remote Sens Spatial Inf Sci XXXVIII-1/C22:25–31*
- Roo APJD, Wesseling CG, Deursen WPAV (2002) Physically based river basin modelling within a GIS: The LISFLOOD model. *Hydrol Process* 14:1981–1992
- Sampson CC, Fewtrell TJ, Duncan A, Shaad K, Horritt MS, Bates PD (2012) Use of terrestrial laser scanning data to drive decimetric resolution urban inundation models. *Adv Water Resour* 41:1–17. <https://doi.org/10.1016/j.advwatres.2012.02.010>
- Sayama T, Ozawa G, Kawakami T, Nabesaka S, Fukami K (2012) Rainfall-runoff-inundation analysis of the 2010 Pakistan flood in the Kabul River basin. *Hydrol Sci J* 57:298–312. <https://doi.org/10.1080/02626667.2011.644245>
- Schumann Guy J-P, Muhlhausen J, Andreadis KM (2019) Rapid mapping of small-scale river-floodplain environments using UAV SfM supports classical theory. *Remote Sens* 11:982. <https://doi.org/10.3390/rs11080982>
- Shen D, Wang J, Cheng X, Rui Y, Ye S (2015) Integration of 2-D hydraulic model and high-resolution lidar-derived DEM for floodplain flow modeling. *Hydrol Earth Syst Sci* 19:3605–3616. <https://doi.org/10.5194/hess-19-3605-2015>
- Shepard D (1968) A two-dimensional interpolation function for irregularly-spaced data. In Proceedings of the 1968 23rd ACM national conference, pp. 517–524

- Shortridge A, Messina J (2011) Spatial structure and landscape associations of SRTM error. *Remote Sens Environ* 115:1576–1587. <https://doi.org/10.1016/j.rse.2011.02.017>
- Sithole G, Vosselman G (2004) Experimental comparison of filter algorithms for bare-Earth extraction from airborne laser scanning point clouds. *ISPRS J Photogramm Remote Sens* 59:85–101. <https://doi.org/10.1016/j.isprsjprs.2004.05.004>
- Sithole G, Vosselman G (2006) Bridge detection in airborne laser scanner data. *ISPRS J Photogramm Remote Sens* 61:33–46. <https://doi.org/10.1016/j.isprsjprs.2006.07.004>
- Turner AB, Colby JD, Csontos RM, Batten M (2013) Flood modelling using a synthesis of multi-platform LiDAR data. *Water* 5:1533–1560. <https://doi.org/10.3390/w5041533>
- Vosselman G (2000) Slope based filtering of laser altimetry data. *IAPRS Int Arch Photogramm Remote Sens Spatial Inf Sci* 33:935–942
- Wang Y, Zheng T (2005) Comparison of light detection and ranging and nation elevation dataset digital elevation model on floodplains of North Carolina. *Nat Hazards Rev* 6:34–40. [https://doi.org/10.1061/\(ASCE\)1527-6988\(2005\)6:1\(34\)](https://doi.org/10.1061/(ASCE)1527-6988(2005)6:1(34))
- Westoby J, Brasington J, Glasser F, Hambrey J, Reynolds M (2012) Structure from-motion photogrammetry: a low-cost, effective tool for geoscience applications. *Geomorphology (amst)* 179:300–314. <https://doi.org/10.1016/j.geomorph.2012.08.021>
- Xia X, Liang Q, Ming X (2019) A full-scale fluvial flood modelling framework based on a high-performance integrated hydrodynamic modelling system (HiPIMS). *Adv Water Resour* 132:103392. <https://doi.org/10.1016/j.advwatres.2019.103392>
- Yalcin E (2019) Two-dimensional hydrodynamic modelling for urban flood risk assessment using unmanned aerial vehicle imagery: a case study of Kirsehir. *Turkey J Flood Risk Management* 12(Suppl. 1):e12499. <https://doi.org/10.1111/jfr3.12499>
- Yan K, Di Baldassarre G, Solomatine DP (2013) Exploring the potential of SRTM topographic data for flood inundation modelling under uncertainty. *J Hydroinform* 15:849–861. <https://doi.org/10.2166/hydro.2013.137>
- Yu D (2010) Parallelization of a two-dimensional flood inundation model based on domain decomposition. *Environ Model Softw* 25:935–945. <https://doi.org/10.1016/j.envsoft.2010.03.003>
- Xing Y, Liang Q, Wang G, Ming X, Xia X (2019) City-scale hydrodynamic modelling of urban flash floods: the issues of scale and resolution. *Nat Hazards* 96:473–496. <https://doi.org/10.1007/s11069-018-3553-z>
- Zazo S, Molina JL, Rodríguez-González P (2015) Analysis of flood modeling through innovative geometric methods. *J Hydrol* 524:522–537. <https://doi.org/10.1016/j.jhydrol.2015.03.011>
- Zhang Q, Chen C, Whitman D, Shyu L, Yan H, Zhang C (2003) A progressive morphological filter for removing non ground measurements from airborne LiDAR data. *IEEE Trans Geosci Remote Sens* 41(4):872–882. <https://doi.org/10.1109/TGRS.2003.810682>
- Zhang Y, Crawford P (2020) Automated extraction of visible floodwater in dense urban areas from RGB aerial photos. *Remote Sens* 12:2198. <https://doi.org/10.3390/rs12142198>
- Zhang J, Lin X, Ning X (2013) SVM-based classification of segmented airborne Lidar point clouds in urban areas. *Remote Sens* 2013:3749–3775. <https://doi.org/10.3390/rs5083749>
- Zhao G, Balstrøm T, Mark O, Jensen MB (2021) Multi-scale target-specified sub-model approach for fast large-scale high-resolution 2D urban flood modelling. *Water* 13:259. <https://doi.org/10.3390/w13030259>